Double-layer stochastic model predictive voltage control in active distribution networks with high penetration of renewables

Zhang, Zhengfa; Silva, Filipe Miguel Faria da; Guo, Yifei; Bak, Claus Leth; Chen, Zhe

Published in:
Applied Energy

DOI (link to publication from Publisher):
10.1016/j.apenergy.2021.117530

Publication date:
2021

Document Version
Publisher's PDF, also known as Version of record

Applied Energy 302 (2021) 117530

Contents lists available at ScienceDirect

Applied Energy

journal homepage: www.elsevier.com/locate/apenergy

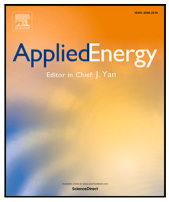

Double-layer stochastic model predictive voltage control in active distribution networks with high penetration of renewables ☆

Zhengfa Zhang [a,*], Filipe Faria da Silva [a], Yifei Guo [b], Claus Leth Bak [a], Zhe Chen [a]

[a] Department of Energy Technology, Aalborg University, Aalborg 9220, Denmark
[b] Department of Electrical and Electronic Engineering, Imperial College, London SW7 2AZ, UK

ARTICLE INFO

Keywords:
Voltage/var control
Stochastic model predictive control
Distribution network
Distributed generation
Double-layer control

ABSTRACT

The high penetration of renewable energy into distribution networks poses increasing challenges on voltage control. To address this issue, this paper presents a double-layer stochastic model predictive control algorithm to regulate voltage profile in active distribution networks. In the proposed algorithm, voltage regulation is achieved by coordination of an upper layer controller and a lower layer controller. In the upper layer, the number of operation of mechanical voltage regulation devices, including transformer with on-load tap changer and capacitor banks, is minimized in an hourly timescale. In the lower layer, the controller minimizes the active power curtailments and power losses with a control period of 5 min. The proposed double-layer stochastic model predictive voltage control utilizes not only the reactive power control, but also the active power curtailment to regulate bus voltages. In addition, mechanical voltage regulation devices and distributed generations are controlled in two different timescales. Case studies on a modified IEEE-33 bus system demonstrate that compared with traditional control and two-stage stochastic voltage control, the proposed algorithm can achieve an improvement of 8.05% and 7.43%, respectively.

1. Introduction

In recent decades, motivated by environmental protection and energy-saving policy, the share of renewable energy is growing rapidly around the world [1]. Especially, an increasing proportion of renewable-based distributed generations (DGs), such as photovoltaic panels and wind turbines, has been integrated into distribution networks (DNs) [2]. Due to its inherent uncertainty and variability, the increasing penetration of renewable energy poses a variety of challenges on the secure and reliable operation of DNs, with voltage control being one of them [3].

The main purpose of voltage/var control (VVC) is to maintain the voltage profile within an acceptable range. Conventionally, VVC is achieved by utility-owned mechanical VVC devices, such as transformers with on-load tap changer (OLTC), step voltage regulators (SVRs) and switchable capacitor banks(CBs), of which the lifespan is related with the number of their operations. Due to the intermittent and fluctuating nature, the high penetration of renewable-based DGs often leads to larger voltage variation or even reversed power flow, making VVC more complicated than ever before. Limited by slow response speed, mechanical VVC devices are less effective in regulating voltages in presence of high-penetration of DGs. Furthermore, regulating voltages under scenarios with high penetrated renewables requires more frequent operation of the mechanical devices, which dramatically reducing their lifetime. Therefore, the power electronics interfaced DGs with fast and continuous characteristics are encouraged to provide additional voltage support [4].

The existing works on VVC mainly fall into two groups: rule-based and optimization-based methods. In rule-based methods, VVC devices respond to local measurements by pre-defined rules. Among them, the most commonly adopted one is droop control as advocated by IEEE 1547 Standard [4]. Other approaches include proportional and integral control [5], or other customized control curves, such as delayed voltage droop [6], adaptive control [7] and hybrid local control [8]. Although fast and simple to implement, rule-based methods cannot guarantee system-wide optimization and overall stability, because of their local nature. By contrast, optimization-based methods formulate the decision making process as a non-convex optimal power flow (OPF) problem by gathering system-wide information such as network parameters, nodal load and generation. Particle swarm optimization (PSO) [9], genetic algorithm (GA) [10] and evolutionary algorithm (EA) [11] were used, respectively, to realize certain objectives such as network losses

☆ This work is supported by China Scholarship Council and Department of Energy Technology, Aalborg University.
* Corresponding author.
E-mail address: zhf@et.aau.dk (Z. Zhang).

https://doi.org/10.1016/j.apenergy.2021.117530
Received 23 March 2021; Received in revised form 23 July 2021; Accepted 30 July 2021
Available online 13 August 2021

Nomenclature

Abbreviations

APC	Active power curtailment
CB	Capacitor bank
DG	Distributed generation
DL-SMPC	Double-layer stochastic model predictive control
DN	Distribution network
EA	Evolutionary algorithm
GA	Genetic algorithm
LLC	Lower layer controller
MPC	Model predictive control
OLTC	On-load tap changer
OPF	Optimal power flow
PCC	Point of common coupling
PSO	Particle swarm optimization
SDP	Semi-definite programming
SMPC	Stochastic model predictive control
SOCP	Second order cone programming
SVR	Step voltage regulator
TS-VVC	Two-stage stochastic VVC
ULC	Upper layer controller
VVC	Voltage/var control

Parameters

$\boldsymbol{a}_0^T$	First row of graph incidence matrix
$\boldsymbol{R}$, $\boldsymbol{X}$	DN resistance/reactance diagonal matrix of set $\mathcal{L}$
c_{tap}, c_c, c_p	Cost coefficients of OLTC and CB operation, active power losses
S_g	DG rated capacity
α, β	Shape parameters of Beta distribution
$\bar{\boldsymbol{A}}$	Graph incidence matrix of DN topology
$\boldsymbol{A}$	Submatrix of graph incidence matrix $\bar{\boldsymbol{A}}$
$\boldsymbol{C}_g$, $\boldsymbol{C}_c$	Mapping matrix between DG/CB incidence and buses
$\boldsymbol{n}_c^{max}$, $\boldsymbol{n}_c^{min}$	CB maximum/mimimun tap position
$\boldsymbol{n}_{tap}^{max}$, $\boldsymbol{n}_{tap}^{min}$	OLTC maximum/mimimun tap position
Δtap	OLTC voltage changer per step
ω_{mec}, ω_p	Weighting factors for mechanical VVC devices operation and active power losses
ρ_s	Probability of scenario $s \in \mathcal{S}$
$\Delta\boldsymbol{n}_c^{max}$, $\Delta\boldsymbol{n}_c^{min}$	CB maximum/mimimun ramping limit
$\Delta\boldsymbol{n}_{tap}^{max}$, $\Delta\boldsymbol{n}_{tap}^{min}$	OLTC maximum/mimimun ramping limit
Δq_c	CB reactive power per step
N_p	Prediction step
N_k	Number of LSC control steps in T_c
P_{max}	DG maximum available active power
r_{ij}, x_{ij}	Branch resistance/reactance at branch (i, j)
T_c, t_c	Control period of upper/lower layer controller
V_{max}, V_{min}	Voltage maximum/mimimun limit

Sets

$\mathcal{L}$	Set of branches
$\mathcal{N}$	Set of buses
$\mathcal{N}_c$	Set of CBs
$\mathcal{N}_g$	Set of DGs
$\mathcal{S}$	Set of stochastic scenarios

Variables

$\boldsymbol{V}$	Vector of voltage magnitude of all buses
p_j^g, q_j^g	Real/reactive power output from DG inverters
p_j^l, q_j^l	Load real/reactive power consumption
q_j^c	Reactive power injection from capacitor bank
$\boldsymbol{n}_{tap}$, $\boldsymbol{n}_c$	Vector of OLTC/CB tap position
$\boldsymbol{p}$, $\boldsymbol{q}$	Vector of real/reactive power injection of set $\mathcal{N}$
$\boldsymbol{P}$, $\boldsymbol{Q}$	Vector of real/reactive power of set $\mathcal{L}$
$\boldsymbol{p}_l$, $\boldsymbol{q}_l$	Vector of real/reactive power consumption of set $\mathcal{N}$
$\boldsymbol{p}_g$, $\boldsymbol{q}_g$	Vector of real/reactive power output of set $\mathcal{N}_g$
$\boldsymbol{q}_c$	Vector of reactive power injection of set $\mathcal{N}_c$
P_{ij} ,Q_{ij}	Real/reactive power from bus i to bus j
p_j, q_j	Real/reactive power injection at bus j
P_{cur}	Active power curtailments of all DGs
P_{loss}	Network power losses

minimization, voltage profile improvement, OLTC operation reduction, etc. However, these heuristic methods suffer from heavy computational burden, inconsistent solutions and slow convergence. Other methods attempted to transform the non-convex models into convex ones using linear approximation or convex relaxations such as second-order cone programming (SOCP) relaxation [12] and semi-definite programming (SDP) relaxation [13], by which the global optima can be possibly solved. In [12], power distribution systems were formed as a convex SOCP model, then the network losses were minimized in a decentralized manner. In [13], the SDP formulation was used to mitigate voltage problem by collaboration of OLTC and electric vehicles. Furthermore, some works decomposed the control strategy into multiple timescales, considering the different characteristics of VVC devices. In [14], OLTC transformer and CBs were coordinated in two different timescales to minimize voltage deviation and energy losses. In [15], conservation voltage reduction is achieved by coordination of slow-dispatch of OLTC and CBs and fast-dispatch of photovoltaic inverters.

Above works are based on deterministic optimization without considering some inevitable forecasting errors. Stochastic programming is a widely accepted method in addressing voltage issue under uncertainties. In [16], stochastic programming was used to handle uncertainties involving variable load. A scenario-based stochastic model is formulated in [17] to schedule energy storage systems and DGs in order to minimize operation cost. In [18], a two-stage stochastic framework was formulated and chance constrained optimization was used to handle nodal power uncertainties. However, the objective function of the above listed stochastic methods mainly focused on one specific time instant rather than the whole control period. Besides, the decisions are made only relying on the system current status, future control objectives and information are ignored in these one-step optimization.

Due to its multi-step optimization principle and close-loop nature, model predictive control (MPC) for VVC has received attention recently. In [19], MPC was used to regulate voltages via coordination of photovoltaic and energy storage. In [20], the coordination of OLTC, DG units and energy storage system was achieved in a single stage MPC. Therefore, considering the advantages of stochastic programming and MPC, stochastic model predictive control (SMPC) can be a possible

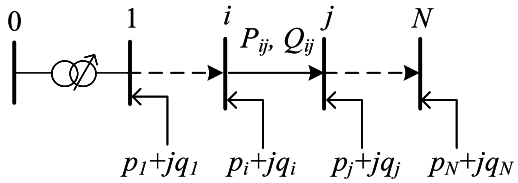

Fig. 1. Topology of a typical radial DN.

solution for time-series VVC under uncertainty. In [21], the OLTC and CBs were scheduled with SMPC by taking into account of the wind and photovoltaic generation prediction error. Ref. [22] proposed a chance constrained SMPC formulation to achieve trade off between control cost reduction and voltage regulation. However, voltage control is performed on one timescale and active power curtailment (APC) is not considered in these recent SMPC works. In fact, voltage magnitudes are sensitive to active power in DNs, due to the high R/X ratio. Besides, DG available reactive power is limited by the instantaneous real power generation and DG capability. Reactive power control alone may be insufficient to regulate voltages, especially when DG has high active power outputs [23].

To fill the research gap of the above works, this paper proposes a double-layer stochastic model predictive control (DL-SMPC) VVC scheme to regulate voltage profile in DN with high penetration of DGs. Compared with the existing works, the main contributions of this paper are summarized as follows:

- The proposed method follows timescale decomposition concept, in which OLTC transformer and CBs with slow response speed are scheduled in the upper layer with a longer control period, whereas DG real and reactive power outputs are dispatched in the lower stage in faster control period.
- The excessive use of OLTC transformer and CBs is reduced in the upper layer to prolong their lifetime, while network power losses and APC are minimized in the lower layer. The limited DG reactive power regulating capability is further compensated by active power control, which is a solution different from most existing works.
- Compared with current SMPC works, the proposed DL-SMPC utilizes not only the reactive power control, but also the active power curtailment to regulate the bus voltages. In addition, the mechanical VVC devices and DGs are controlled in two timescales, considering their different response speed.

The rest of this paper is organized as follows: Section 2 briefly describes system modelling. Section 3 introduces the formulation of the proposed algorithm. Simulation results are presented in Section 4 followed by conclusions.

2. System modelling

2.1. Modelling of DN

A typical radial DN with $N+1$ buses is illustrated in Fig. 1. The $N+1$ buses are denoted by set $\mathcal{N}\cup\{0\}$, $\mathcal{N} := \{1,\dots,N\}$ and bus 0 is assumed to be the reference bus. For each bus $j \in \mathcal{N}$, $u_j := V_j^2$ represents the squared voltage magnitude while p_j and q_j are the real and reactive power injection, respectively. The N branches are collected into the set $\mathcal{L}$, for each branch $(i,j) \in \mathcal{L}$, r_{ij} and x_{ij} denote the branch resistance and reactance while P_{ij} and Q_{ij} are real and reactive power from bus i to bus j. The power flow for each branch $(i,j) \in \mathcal{L}$ can be described by Distflow equations [24]:

$$P_{ij} = \sum_{k\in\mathcal{N}_j} P_{jk} - p_j + r_{ij}\ell_{ij} \tag{1a}$$

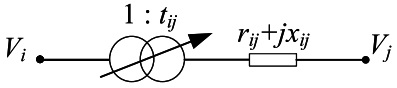

Fig. 2. Branch flow model with OLTC.

$$Q_{ij} = \sum_{k\in\mathcal{N}_j} Q_{jk} - q_j + x_{ij}\ell_{ij} \tag{1b}$$

$$u_i - u_j = 2\left(r_{ij}P_{ij} + x_{ij}Q_{ij}\right) - \left(r_{ij}^2 + x_{ij}^2\right)\ell_{ij} \tag{1c}$$

$$\ell_{ij} = \frac{P_{ij}^2 + Q_{ij}^2}{u_i} \tag{1d}$$

$$p_j = p_j^g - p_j^l \tag{1e}$$

$$q_j = q_j^g + q_j^c - q_j^l \tag{1f}$$

where p_j^g and q_j^g are real/reactive power from DG inverters, p_j^l and q_j^l are the load real/reactive power consumption, q_j^c is reactive power injection from CB.

The existence of ℓ_{ij} makes above equations nonconvex. Given the fact that ℓ_{ij} is negligible compared with the linear terms, and DN has a relatively flat voltage profile, (1a)–(1c) can be approximated into a linear Distflow model, such approximation introduces a small modelling error at about 0.25%(1%) if there is a 5%(10%) deviation in voltage magnitude [25]. The linear model can be represented as,

$$P_{ij} = \sum_{k\in\mathcal{N}_j} P_{jk} - p_j \tag{2a}$$

$$Q_{ij} = \sum_{k\in\mathcal{N}_j} Q_{jk} - q_j \tag{2b}$$

$$V_i - V_j = r_{ij}P_{ij} + x_{ij}Q_{ij} \tag{2c}$$

For branch (i,j) with OLTC transformer, the on-load tap changer is assumed to be on the secondary side of the transformer as shown in Fig. 2, so (2c) can be reformed as,

$$t_{ij}V_i - V_j = r_{ij}P_{ij} + x_{ij}Q_{ij} \tag{2d}$$

where $t_{ij} = 1 + n_{tap}\Delta tap$, $n_{tap,ij}$ and Δtap_{ij} denote OLTC tap position and voltage change per step, respectively.

2.2. Compact form representation of linear Distflow model

In order to implement the numerical algorithms efficiently, the compact form of linear Distflow model is introduced in this section. Firstly, voltage magnitudes in set $\mathcal{N}$, real/reactive power flow in set $\mathcal{L}$ are collected into column vectors $\boldsymbol{V}$, $\boldsymbol{P}$ and $\boldsymbol{Q}$. The load real and reactive power consumption in bus set $\mathcal{N}$ are collected as $\boldsymbol{p}_l := \left[p_1^l,\dots,p_N^l\right]^\top$, $\boldsymbol{q}_l := \left[q_1^l,\dots,q_N^l\right]^\top$. Let $\mathcal{N}_g := \{1,\dots,n\}$ denote the set of DGs and define real/reactive power injection from DGs as $\boldsymbol{p}_g := \left[p_1^g,\dots,p_n^g\right]^\top$, $\boldsymbol{q}_g := \left[q_1^g,\dots,q_n^g\right]^\top$, respectively. Similarly, let $\mathcal{N}_c := \{1,\dots,m\}$ denote the set of CBs and $\boldsymbol{q}_c := \left[q_1^c,\dots,q_m^c\right]^\top$ denote the reactive power injection from CBs. Let $\boldsymbol{C}_g \in \mathbb{R}^{N\times n}$ denote the mapping matrix between DG incidence and the buses, which is defined as: the element at the ith row, jth column of $\boldsymbol{C}_g$ is 1 if DG $j \in \mathcal{N}_g$ is located at bus i. The mapping matrix between CB incidence and the buses $\boldsymbol{C}_c \in \mathbb{R}^{N\times m}$ is also defined in the same way. Then the vector of real/reactive power injection of set $\mathcal{N}$ can be denoted as $\boldsymbol{p} := \left[p_1,\dots,p_N\right]^\top = \boldsymbol{C}_g\boldsymbol{p}_g - \boldsymbol{p}_l$ and $\boldsymbol{q} := \left[q_1,\dots,q_N\right]^\top = \boldsymbol{C}_g\boldsymbol{q}_g + \boldsymbol{C}_c\boldsymbol{q}_c - \boldsymbol{q}_l$, respectively.

Let $\bar{\boldsymbol{A}} := \left[\boldsymbol{a}_0\ \boldsymbol{A}^\top\right]^\top \in \{0,\pm1\}^{(N+1)\times N}$ denotes the incidence matrix of DN topology graph [26], $\boldsymbol{a}_0^\top$ is the first row of $\bar{\boldsymbol{A}}$ and $\boldsymbol{A}$ is the remaining submatrix. Define diagonal matrices $\boldsymbol{R} := \mathrm{diag}\left(\{R_l\}\right) \in \mathbb{R}^{N\times N}$ with ℓ_th diagonal element equals to r_{ij} of ℓ_th branch $\in \mathcal{L}$, the same is

with $\boldsymbol{X} := \mathrm{diag}\left(\{X_l\}\right) \in \mathbb{R}^{N\times N}$. Then the compact form of (2a)–(2c) can be represented as,

$$-\boldsymbol{AP} = \boldsymbol{p} \tag{3a}$$

$$-\boldsymbol{AQ} = \boldsymbol{q} \tag{3b}$$

$$\begin{bmatrix}\boldsymbol{a}^0 & \boldsymbol{A}^\top\end{bmatrix}\begin{bmatrix}\boldsymbol{V}_0 \\ \boldsymbol{V}\end{bmatrix} = \boldsymbol{RP} + \boldsymbol{XQ} \tag{3c}$$

By substituting (3a), (3b) and (2d) into (3c), we have,

$$\boldsymbol{V} = \boldsymbol{D}_r\boldsymbol{p} + \boldsymbol{D}_x\boldsymbol{q} - \boldsymbol{A}^{-\top}\boldsymbol{a}_0\left(1 + \boldsymbol{n}_{tap}\Delta\boldsymbol{tap}\right) \tag{4}$$

where $\boldsymbol{D}_r := \boldsymbol{A}^{-\top}\boldsymbol{R}\boldsymbol{A}^{-1}$ and $\boldsymbol{D}_x := \boldsymbol{A}^{-\top}\boldsymbol{X}\boldsymbol{A}^{-1}$. (4) can be equivalently given as,

$$\begin{aligned}\boldsymbol{V} =& \boldsymbol{D}_r\left(\boldsymbol{C}_g\boldsymbol{p}_g - \boldsymbol{p}_l\right) + \boldsymbol{D}_x\left(\boldsymbol{C}_g\boldsymbol{q}_g + \boldsymbol{C}_c\boldsymbol{q}_c - \boldsymbol{q}_l\right) \\ & - \boldsymbol{A}^{-\top}\boldsymbol{a}_0\left(1 + \boldsymbol{n}_{tap}\Delta\boldsymbol{tap}\right) \\ =& \boldsymbol{D}_r\boldsymbol{C}_g\boldsymbol{p}_g + \boldsymbol{D}_x\left(\boldsymbol{C}_g\boldsymbol{q}_g + \boldsymbol{C}_c\boldsymbol{q}_c\right) \\ & - \boldsymbol{A}^{-\top}\boldsymbol{a}_0\boldsymbol{n}_{tap}\Delta\boldsymbol{tap} + \overline{\boldsymbol{V}}\end{aligned} \tag{5}$$

where $\overline{\boldsymbol{V}} = -\boldsymbol{D}_r\boldsymbol{p}_l - \boldsymbol{D}_x\boldsymbol{q}_l - \boldsymbol{A}^{-\top}\boldsymbol{a}_0$ denotes voltage profile under no control action.

3. Two-stage stochastic MPC algorithm

The algorithm of two-stage SMPC is introduced in this section, including the modelling of uncertainty from the generation and load, the idea of two-stage SMPC and how to reformulate the problem into its deterministic equivalent.

3.1. Scenario generation

The uncertainty associated with the generation and load is indicated by forecasting errors from their predictive values. Beta distribution [27] and normal distribution [21] are widely accepted probability distribution functions to represent the predictive errors of generation and load, respectively, and are therefore used in this paper.

Beta distribution is located on the interval [0,1] and its probability density function is defined by two shape parameters α and β. For a given predicted power $\hat{P}$, the occurrence of real value x can be represented by,

$$f_{\hat{P}}(x) = x^{\alpha-1}\cdot(1-x)^{\beta-1}\cdot B(\alpha,\beta) \tag{6}$$

where $B(\alpha,\beta)$ is normalized factor to make (6) integrate to 1. The relationship of α and β with the mean value $\bar{P}$ and variance values σ^2 are as follows,

$$\bar{P} = \frac{\hat{P}}{S_g} = \frac{\alpha}{\alpha+\beta} \tag{7a}$$

$$\sigma^2 = \frac{\alpha\cdot\beta}{(\alpha+\beta)^2\cdot(\alpha+\beta+1)} \tag{7b}$$

where S_g is the DG rated capacity, $\hat{P}$ is the predicted DG power output and $\bar{P}$ denotes the normalized DG power output. For a given predicted generation, shape parameters can be calculated using (7). For the load, the mean value of normal distribution is the predicted load consumption. After the parameters of beta distribution and normal distribution are determined, Monte-Carlo simulation is employed to generate large number of scenarios to represent the stochastic feather of generation and load.

3.2. Scenario reduction

In scenario-based optimization, the computational burden grows with increasing number of scenarios. Hence, the backward reduction method is used to reduce the scenario number while maintaining a good approximation of the original scenario set.

Suppose a stochastic set S contains K different scenarios, each with probability ρ_s. The distance between two scenario pair (s, s') is defined by

$$d_{s,s'} = \max\left\{1, \|s-\bar{s}\|, \|s'-\bar{s}\|\right\}\left\|s-s'\right\| \tag{8}$$

where $\bar{s}$ is the average value of scenarios and $\|\cdot\|$ denotes the Euclidean distance.

The basic idea of backward reduction is to select the scenario with minimal probability and distance to other scenarios in the scenario set. Then the selected scenario will be eliminated and represented by the scenario closest to it. The process repeats until the required number to be deleted is met [28,29]. The backward reduction method consists of the following steps,

Step 1: Compute the distances of all scenarios pairs $d_{s,s'}$, $s, s' \in S$.

Step 2: For each scenario k, $d_k(r) = \min d_{k,s'}, k, s' \in S$ and $s' \neq k$, r is the scenario index that has the minimum distance with scenario k.

Step 3: Calculate $\rho d_k(r) = \rho_k \times d_k(r)$, $k \in S$. Choose d so that $\rho d_d = \min \rho d_k$, d is the scenario index.

Step 4: $S = S - \{d\}$; $\rho_r = \rho_r + \rho_d$.

Step 5: Repeat step 2 to step 4 until the number of scenarios to be reduced is met.

3.3. Two-stage stochastic MPC

The key idea behind SMPC is to compute an optimal control input while respecting various constraints for all the trajectories determined by the scenario set. In SMPC, the first stage decision variables are determined before the realization of uncertain data, the second stage decision variables are made after knowing the actual realization of each scenario. The general form of two-stage SMPC at each time instant k is as follows,

$$min \sum_{t=k}^{k+N_p-1}\left(f(x(t)) + E\left[Q(x(t),\omega)\right]\right) \tag{9}$$

where N_p is the prediction step, x is the first stage decision variables, ω indicates uncertainty variables with a known probability distribution, $Q(x,\omega)$ is the optimal value of the second stage problem, $E[Q(x,\omega)]$ is the expected value in the second stage.

Scenario-based approach is commonly used to reformulate stochastic programming problem into its deterministic equivalent, in which the continuous random variables are represented by a finite set of scenarios. Thus, (9) can be reformulated as its deterministic counterpart in which each scenario shares the common first stage variables. The reformulated deterministic equivalent problem is given by

$$min\left[\sum_{t=k}^{k+N_p-1}\left(f(x(t)) + \rho_s\cdot\sum_{s\in S} y_s(x(t),\omega)\right)\right] \tag{10}$$

where S denotes a finite number scenario set with each scenario has the probability of ρ_s, y_s denotes the value of second stage problem in each scenario.

4. Formulation of the DL-SMPC

The algorithm of proposed DL-SMPC is illustrated in Fig. 3. In DL-SMPC, there is an upper layer controller(ULC) operated with a slow time period T_c of 1 h and a lower layer controller(LLC) operated at a fast timescale t_c of 5 min. The ULC corresponds to the first stage variables in SMPC while the LLC corresponds to the second stage variables. The ULC is triggered at the beginning of an hour, the expected outcome is the OLTC and CB tap position, as well as the real/reactive DG outputs for the first 5 min. Once the OLTC and CB tap position are obtained, they will keep fix for the whole hour and send to the lower layer controller(LLC). Then LLC decides DG real/reactive power outputs based on the results received from ULC in a shorter time period of 5 min.

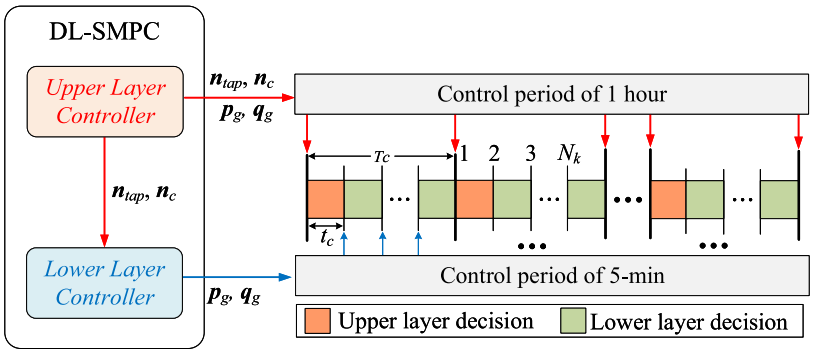

Fig. 3. DL-SMPC framework.

4.1. Upper layer controller

The main objective of the ULC is to reduce the number of OLTC and CB operation to prolong their lifetime, as well as to minimize the network power losses and active power curtailments. The power losses and active power curtailments are both active power cost from the perspective of distribution system operator, so the sum of the both are termed as active power losses in this paper. The mathematical formulation of ULC at time instant k is expressed as,

$$min \sum_{t=k}^{k+N_p-1} \begin{bmatrix} \omega_{mec} \cdot \left(\begin{matrix} c_{tap} \left| \boldsymbol{n}_{tap}(t) - \boldsymbol{n}_{tap}(t-1) \right| \\ +c_c \left| \boldsymbol{n}_c(t) - \boldsymbol{n}_c(t-1) \right| \end{matrix} \right) + \\ \omega_p \cdot \rho_s \sum_{s \in S} \sum_{i=k}^{k+N_k-1} c_p \left(P_{cur,s}(i) + P_{loss,s}(i) \right) \end{bmatrix} \tag{11}$$

over $\forall (i,j) \in \mathcal{L}, \forall i,\ j \in \mathcal{N}, \forall k \in \{1, 2 \cdots N_p\}$
subject to,

$$P_{ij}(k) - \sum_{k \in \mathcal{N}_j} P_{jk}(k) = -p_j(k) \tag{12}$$

$$Q_{ij}(k) - \sum_{k \in \mathcal{N}_j} Q_{jk}(k) = -q_j(k) \tag{13}$$

$$V_i(k) - V_j(k) = r_{ij} P_{ij}(k) + x_{ij} Q_{ij}(k) \tag{14}$$

$$V_1 = V_0 \left(1 + n_{tap}(k) \Delta tap\right) \tag{15}$$

$$V_{min} \leqslant V_i(k) \leqslant V_{max} \tag{16}$$

$$P_{loss}(k) = \sum_{(i,j) \in \mathcal{L}} r_{ij} \frac{P_{ij}^2(k) + Q_{ij}^2(k)}{V_0^2} \tag{17}$$

$$\boldsymbol{n}_{tap}^{min} \leqslant \boldsymbol{n}_{tap}(k) \leqslant \boldsymbol{n}_{tap}^{max} \tag{18}$$

$$\Delta \boldsymbol{n}_{tap}^{min} \leqslant \left| \boldsymbol{n}_{tap}(k) - \boldsymbol{n}_{tap}(k-1) \right| \leqslant \Delta \boldsymbol{n}_{tap}^{max} \tag{19}$$

$$\boldsymbol{q}_c(k) = \boldsymbol{n}_c(k) \cdot \Delta q_c \tag{20}$$

$$\boldsymbol{n}_c^{min} \leqslant \boldsymbol{n}_c(k) \leqslant \boldsymbol{n}_c^{max} \tag{21}$$

$$\Delta \boldsymbol{n}_c^{min} \leqslant \left| \boldsymbol{n}_c(k) - \boldsymbol{n}_c(k-1) \right| \leqslant \Delta \boldsymbol{n}_c^{max} \tag{22}$$

$$0 \leqslant \boldsymbol{p}_g(k) \leqslant \boldsymbol{P}_{max}(k) \tag{23}$$

$$\boldsymbol{P}_{cur}(k) = \boldsymbol{P}_{max}(k) - \boldsymbol{p}_g(k) \tag{24}$$

$$\left| \boldsymbol{q}_g(k) \right| \leqslant \sqrt{\boldsymbol{S}_g^2 - \boldsymbol{p}_g^2(k)} \tag{25}$$

$$N_k = T_c / t_c \tag{26}$$

where $\boldsymbol{n}_{tap}$ and $\boldsymbol{n}_c$ are vectors of the OLTC and CB position, respectively. P_{loss} and P_{cur} are network power losses and total active power curtailments of all DGs, respectively. N_k is the number of LLC control steps within an ULC control interval. (12)–(17) represent power flow constraints, where V_{max} and V_{min} are the voltage limits. (18)–(19) denote operation constraints of OLTC transformer. In (20), the CBs are modelled as reactive power sources with integer number to indicate their discrete characteristics, (21)–(22) represent CB operation constraints. (23)–(25) represent the constraints for DG inverter operation, in which $\boldsymbol{p}_g$ and $\boldsymbol{q}_g$ denotes the vectors of DG real/reactive power output, $\boldsymbol{S}_g$ denotes DG rated capability and $\boldsymbol{P}_{max}$ denotes its maximum available active power. ω_{mec}, ω_p are weighting factors for operation of mechanical devices and active power losses, respectively. The algorithm will have better performance in number of OLTC and CB operation reduction with higher ω_{mec}, whereas have better performance in active power losses reduction with larger ω_p. The weighting factors can be determined by using the analytical hierarchy process(AHP) method [30]. It depends on the need of decision maker and it can vary from network to network in real practice. c_{tap}, c_c and c_p are cost coefficients for operation of OLTC and CB as well as active power losses.

(12)–(17) are not in the form of compact representation. To implement the proposed DL-SMPC efficiently, (12)–(17) can be reformulated into compact form according to the description in 2.2,

$$\boldsymbol{p}(k) = \boldsymbol{C}_g \boldsymbol{p}_g(k) - \boldsymbol{p}_l(k) \tag{27}$$

$$\boldsymbol{q}(k) = \boldsymbol{C}_g \boldsymbol{q}_g(k) + \boldsymbol{C}_c \boldsymbol{n}_c(k) \Delta \boldsymbol{q}_c - \boldsymbol{q}_l(k) \tag{28}$$

$$-\boldsymbol{A}\boldsymbol{P}(k) = \boldsymbol{p}(k) \tag{29}$$

$$-\boldsymbol{A}\boldsymbol{Q}(k) = \boldsymbol{q}(k) \tag{30}$$

$$\boldsymbol{V}(k) = \boldsymbol{D}_r \boldsymbol{C}_g \boldsymbol{p}_g(k) + \boldsymbol{D}_x \left(\boldsymbol{C}_g \boldsymbol{q}_g(k) + \boldsymbol{C}_c \boldsymbol{n}_c(k) \Delta \boldsymbol{q}_c \right)$$
$$-\boldsymbol{A}^{-\top} \boldsymbol{a}_0 \boldsymbol{n}_{tap}(k) \Delta \boldsymbol{tap} + \bar{\boldsymbol{V}} \tag{31}$$

$$\boldsymbol{V}_{min} \leqslant \boldsymbol{V}(k) \leqslant \boldsymbol{V}_{max} \tag{32}$$

where $\boldsymbol{p}_g(k)$, $\boldsymbol{q}_g(k)$, $\boldsymbol{n}_c(k)$ and $\boldsymbol{n}_{tap}(k)$ are vectors of DG real/reactive power output, CB and OLTC tap positions that to be determined.

4.2. Lower layer controller

The LLC receives OLTC and CB position from ULC, so only DG real/reactive power dispatch is calculated in this step. The response time for a typical power electronics inverter is measured in milliseconds, which is much smaller than control period of LLC(5-min in this study), so the ramping limit for DG real/reactive power output can be ignored, and LLC control actions between two time instants are independent with each other. In the lower layer control at time instant k, $\boldsymbol{n}_{tap}(k) = \boldsymbol{n}_{tap}(T_c)$, $\boldsymbol{n}_c(k) = \boldsymbol{n}_c(T_c)$, where $\boldsymbol{n}_{tap}(T_c)$ and $\boldsymbol{n}_c(T_c)$ are OLTC tap position and CB position received from ULC. So the OLTC transformer and CB operation constraints (18)–(19), (20)–(22) in ULC are omitted here. Thus, the mathematical formulation of LLC for time instant k is expressed as follows,

$$min \left[\rho_s \sum_{s \in S} \left(P_{cur,s}(k) + P_{loss,s}(k) \right) \right] \tag{33}$$

over $\forall (i,j) \in \mathcal{L}, \forall i,\ j \in \mathcal{N}, \forall k$,
subject to power flow constraints (12)–(17) and DG inverter operation constraints (23)–(25).

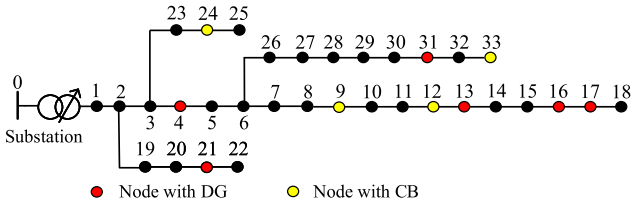

Fig. 4. Topology of modified IEEE-33 bus system.

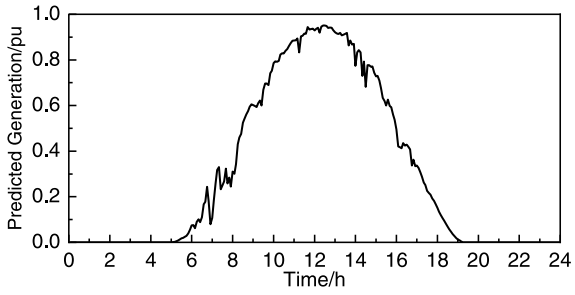

Fig. 5. Predicted PV generation.

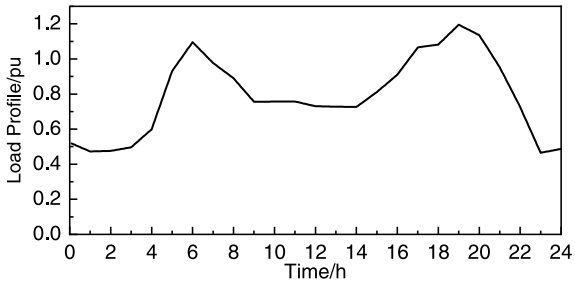

Fig. 6. Load profile.

4.3. Implementing of the proposed DL-SMPC

To better illustrate the proposed methods, the implementing of DL-SMPC is summarized as following,

1. Loading data file containing distribution system information, loading forecasted generation and load data.
2. According to the forecasted value $\bar{P}$ and defined value σ^2, calculate α and β by solving (7). Run Monte Carlo simulation and generate an initial set of scenarios for generation and load using beta distribution and normal distribution. After that, reduce the initial scenario set into a smaller one by backward reduction method.
3. At the beginning of an hour, solve (11) to get the control sequence of OLTC and CB position for the future N_p steps, apply the first in the control sequence while discard the rest, get DG real and reactive power dispatch for the first t_c in an hour.
4. For the rest time of an hour, compute (33) to get the DG real and reactive power outputs according to the OLTC and CB position in step 3.
5. Repeat step 3 and step 4 until the end of the simulation.

5. Case study

5.1. Data and parameters

In this section, the proposed DL-SMPC algorithm is verified on a modified IEEE-33 bus distribution system. The topology of the modified IEEE-33 bus system is shown in Fig. 4 and network parameters can be found in [31]. Case studies are performed in Matlab r2020a with YALMIP Toolbox [32] on an ordinary PC running Win10 with 3.9 Ghz CPU and 16G RAM and the DL-SMPC problem is solved by Gurobi solver [33].

In the studied system, the slack bus voltage is set as 1.02 pu and the maximum/minimum voltage limit are set as 1.05 pu and 0.95 pu, respectively. The OLTC transformer has a ±5% tap range with 20 tap positions, so $\Delta tap = 0.005$, $n_{tap}^{max} = 10$ and $n_{tap}^{min} = -10$. The CBs are installed in bus 9, 12, 24, 33, each with capacity of 300 kVar and 10 tap positions. The ramping limits for OLTC transformer and CBs are assumed to be 1 and 2, respectively. The DGs are located at bus 4, 13, 16, 17, 21, 31, each with capacity of 1.1 MVA. The normalized time-series predicted generation and load profile are obtained from the National Renewable Energy Laboratory (NREL) Renewable Resource Data Center [34], as shown in Figs. 5 and 6, respectively. The prediction horizon is assumed to be 4 h. The mean value for beta distribution and normal distribution is the predicted generation and load while the standard deviation of both probability distribution is assumed to be 5%. The cost coefficient of active power losses is the electricity prize and is set as 0.08 $/kWh, the cost coefficients with the tap change of OLTC and CB are assumed to be 1.40 $ and 0.24 $ per step [35]. Note that above parameters can be adjusted according to real practice. The maximum solution time for ULC problem is 475.14 s and the LLC problem can be solved within 0.66 s. Considering that the time requirements for ULC and LLC are much shorter than the control timescales(1 h for ULC and 5-min for LLC), the implementing of proposed DL-SMPC in real practice can be guaranteed.

5.2. Deterministic VVC

In deterministic VVC, VVC without and with APC is conducted and the necessity of APC is verified. In VVC without APC, DGs always operate at maximum power point tracking(MPPT) mode, and voltages are regulated relying on mechanical VVC devices and DG reactive power adjustments. In contrast, DG real and reactive power are joint dispatched in VVC with APC. The voltage profiles under two simulation are shown in Fig. 7, and DG outputs are shown in Figs. 8 and 9 respectively. For VVC without APC, over-voltage problem occurs at approximately 10:30–14:00, with maximum value reaches 1.09 pu. This is because DG only have limited reactive power capability due to high real power output. Thus, bus voltages cannot be regulated into allowed range even though all DGs absorb reactive power. In contrast, overvoltage issue is properly addressed by joint coordination of real and reactive power control in VVC with APC. During noon time, active power of DGs at bus 13, 16, 17 is curtailed to prevent overvoltage. In addition, due to the APC, DGs at these buses can absorb more reactive power than that in VVC without APC. Therefore, for DN with high penetration of DG, it is not reasonable to keep all DGs operates at MPPT, APC is a necessary for VVC.

5.3. Stochastic VVC

In deterministic VVC, the generation and load are assumed to follow exactly their predicted value. However, in reality, the real value of generation and load could deviate from predicted value due to stochastic weather conditions and consumers behaviour, which highly affect the performance of deterministic VVC. To examine the result of deterministic VVC against uncertainties, 20 random scenarios are generated by Monte Carlo sampling to observe the voltage profiles of all the buses. The voltage profiles for all scenarios at 11:00 are shown in Fig. 10. As can be seen from Fig. 10, overvoltage problem occurs at bus 16, 17 and 18 under approximately 60% scenarios. Then stochastic VVC is performed and the obtained result is verified on the same time instant, as shown in Fig. 11. From Fig. 11 we see that bus voltages are regulated into allowed range under all the test scenarios. Thus, the load and generation stochastic variation need to be taken into consideration in VVC decision making process, in order to guarantee voltage security.

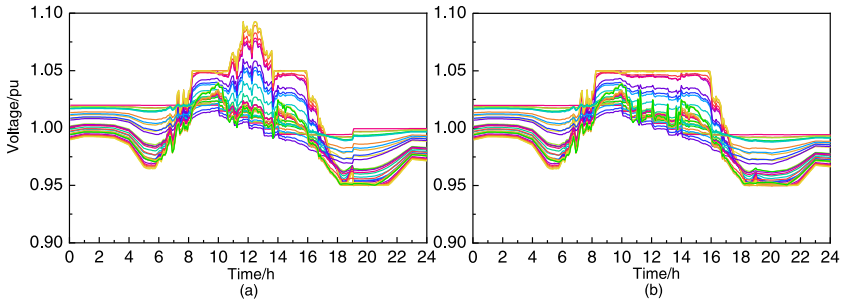

Fig. 7. Voltage profile without (a) and with APC (b).

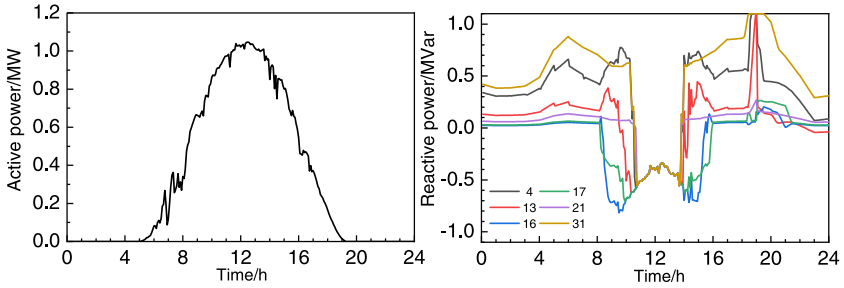

Fig. 8. DG output without APC.

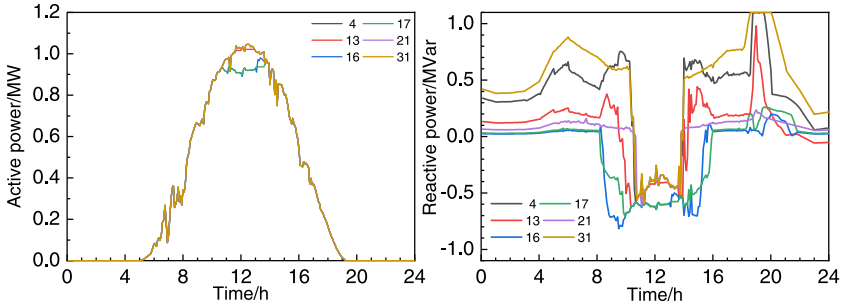

Fig. 9. DG output with APC.

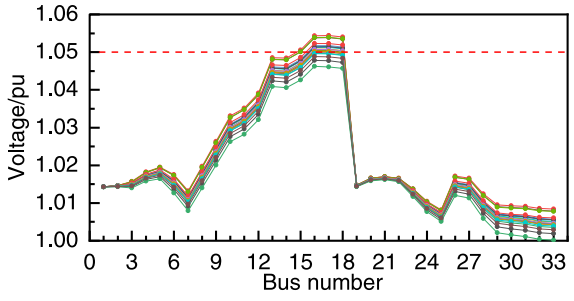

Fig. 10. Performance of deterministic VVC under stochastic scenarios.

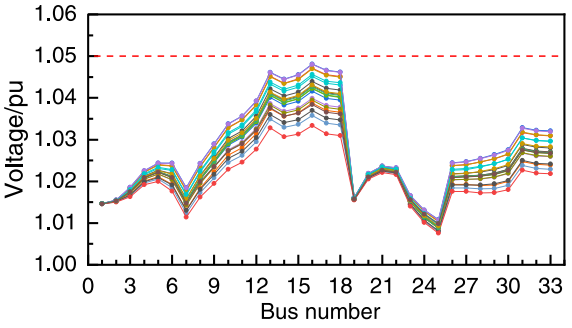

Fig. 11. Performance of stochastic VVC under stochastic scenarios.

5.4. Performance comparison of TS-VVC and DL-SMPC

In this section, a 24-h time-series simulation is conducted and the proposed DL-SMPC is compared with two-stage stochastic VVC(TS-VVC) in which the system future status is not considered. Firstly, 300 random scenarios are generated by Monte Carlo method to represent the stochastic characteristics of generation and load, then the original 300 scenarios are reduced to 30 representative scenarios by backward reduction method. The weighting factors ω_p and ω_{mec} are determined as 0.864 and 0.136 in both methods. The voltage profile, OLTC tap position, CB position and DG real/reactive power output under two simulation are shown in Figs. 12 and 13, respectively. As can be seen from Figs. 12 and 13, both methods are effective in maintaining voltage profiles within allowed range during 24 h. The actions of OLTC and CB position show different patterns in two simulation. The reason for these difference is that the schedule of mechanical devices in TS-VVC only considers control objectives and information at the time instant of the beginning of an hour whereas the DL-SMPC considers control objectives and system status at both the current time instant and the future time

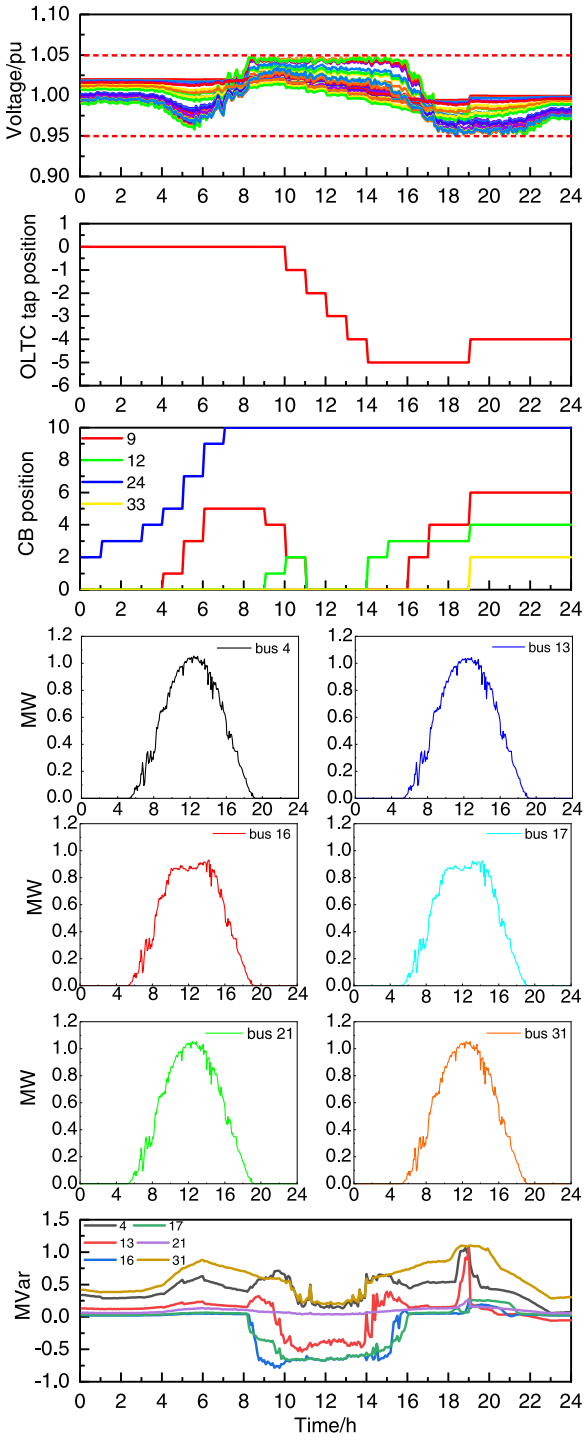

Fig. 12. Time series simulation of TS-VVC.

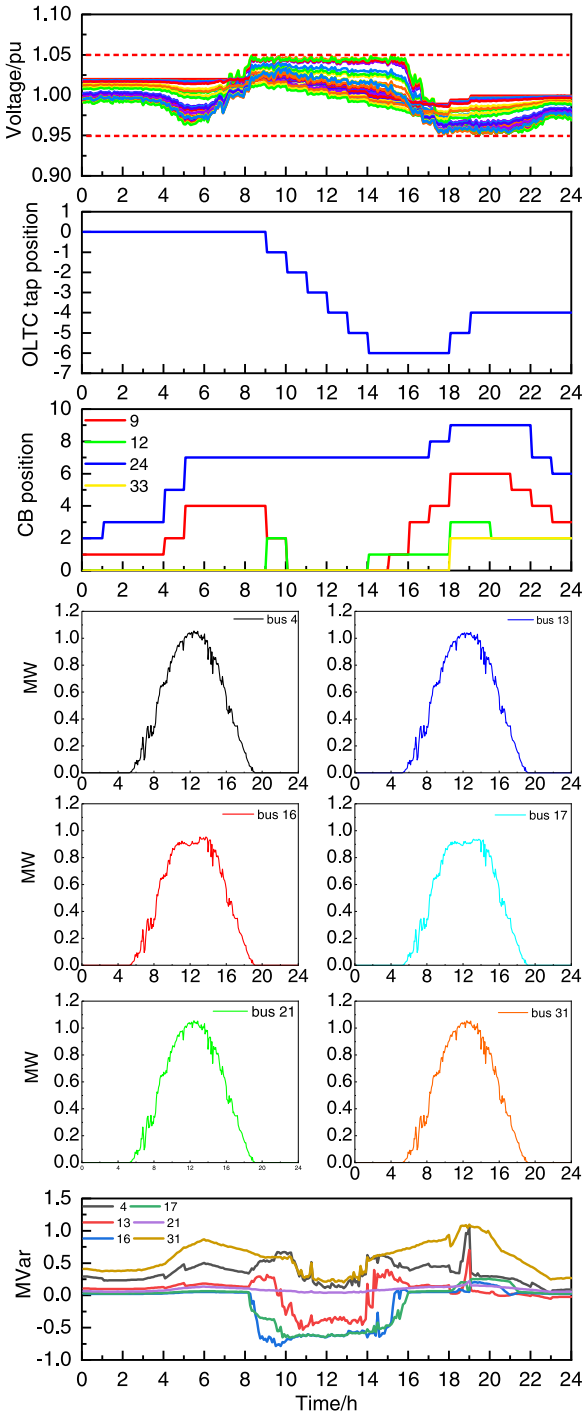

Fig. 13. Time series simulation of DL-SMPC.

interval. During 24 h, DGs located at bus 4, 31 keep operating at MPPT mode, a negligible amount of active power is curtailed for DG located at bus 13 in both simulation. For DGs located at bus 16, 17, the maximum curtailed active power for DGs reaches 0.19 MW in TS-VVC, about 17.3% of DG capability, while that figure is reduced to 0.15 MW in the proposed DL-SMPC simulation. For DG reactive power output, the patterns of two simulation are quite similar with slight difference.

To further demonstrate the effectiveness of the proposed DL-SMPC, the active power losses and the electrical power losses in the whole 24 h are shown in Figs. 14 and 15 respectively. To better illustrate the performance of both methods, traditional OLTC and CB tap control strategy in [36,37] is performed as reference. As shown in Fig. 14, active power losses in DL-SMPC are smaller than in TS-VVC, except some time instants. This is because the DL-SMPC focused more on control objective across the whole period rather than one specific time instant. In Fig. 15, the two curves are quite similar in the first 8 h and begin to deviate after 9:00. The result of comparison is summarized in Table 1. The numbers of OLTC and CB operation in traditional control are 13 and 70, respectively. These numbers are reduced by a lot in both TS-VVC and DL-SMPC. The numbers of OLTC and CB operation in DL-SMPC are slightly higher than that in TS-VVC but almost stay at

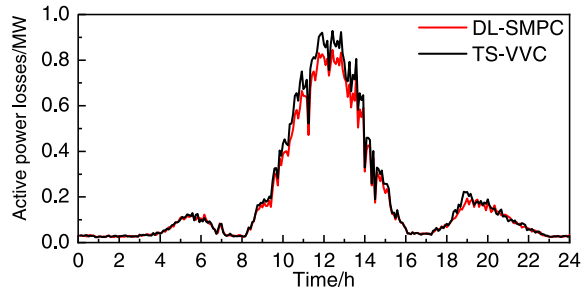

Fig. 14. Active power losses.

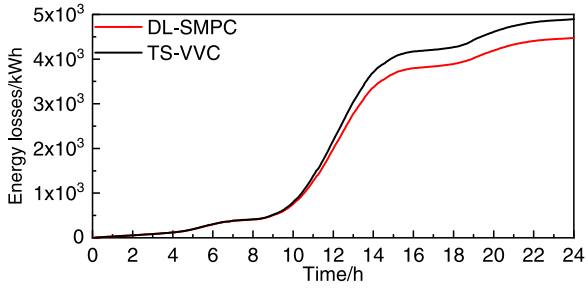

Fig. 15. Energy losses during 24 h.

Table 1
Performance of TS-VVC and DL-SMPC.

	TS-VVC	DL-SMPC	Traditional control
OLTC operation (number of times)	6	8	13
CB operation (number of times)	32	34	70
Energy losses (kWh)	4892.9	4473.5	4697.1
Total cost ($)	408	377.68	410.76

the same level. More importantly, compared with other two methods, the proposed DL-SMPC can achieve fairly improvements in both energy losses(4.76% improvement with traditional control and 8.57% with TS-VVC) and total cost(8.05% with traditional control and 7.43% with TS-VVC). For distribution system operation, rather than one specific time instant, the control objectives would focus more on the whole control period. Thus, the proposed DL-SMPC are more suitable for real distribution system operation.

6. Conclusion

This paper presents a double-layer stochastic model predictive voltage control method to regulate bus voltages in distribution networks with high penetration of renewable based distributed generations. In the proposed method, transformer with on-load tap changer and capacitor banks are scheduled in the upper layer on hourly basis while real and reactive power outputs of distributed generations are dispatched in the lower layer every 5 min. The method aims to reduce the number of operations from mechanical voltage control devices to prolong their lifetime and minimize the active power losses of distributed networks. The proposed double-layer stochastic model predictive voltage control follows time-scale decomposition technology, also the reactive power and active power are comprehensively used to regulate voltage profiles. Compared with stochastic method without considering system future information, there is an improvement of 7.43% in the proposed method. Case studies on a modified IEEE 33 bus system demonstrate the effectiveness of the proposed method. In the future work, the proposed method will be validated on unbalanced distribution networks and using distributed methods.

CRediT authorship contribution statement

Zhengfa Zhang: Methodology, Data curation, Writing – original draft, Software, Validation, Writing – review & editing. **Filipe Faria da Silva:** Supervision, Writing – review & editing. **Yifei Guo:** Methodology, Software. **Claus Leth Bak:** Supervision, Writing – review & editing. **Zhe Chen:** Supervision, Writing – review & editing.

Declaration of competing interest

The authors declare that they have no known competing financial interests or personal relationships that could have appeared to influence the work reported in this paper.

References

[1] Kou Peng, Liang Deliang, Wang Chen, Wu Zihao, Gao Lin. Safe deep reinforcement learning-based constrained optimal control scheme for active distribution networks. Appl Energy 2020;264:114772.
[2] Almasalma Hamada, Claeys Sander, Deconinck Geert. Peer-to-peer-based integrated grid voltage support function for smart photovoltaic inverters. Appl Energy 2019;239:1037–48.
[3] Ehsan Ali, Yang Qiang. Optimal integration and planning of renewable distributed generation in the power distribution networks: A review of analytical techniques. Appl Energy 2018;210:44–59.
[4] Photovoltaics Distributed Generation, Storage Energy. IEEE standard for interconnection and interoperability of distributed energy resources with associated electric power systems interfaces. IEEE Std 2018;1547–2018.
[5] Zhang Baosen, Dominguez-Garcia Alejandro D, Tse David. A local control approach to voltage regulation in distribution networks. In: 2013 North American Power Symposium (NAPS). IEEE; 2013, p. 1–6.
[6] Jahangiri Pedram, Aliprantis Dionysios C. Distributed volt/VAr control by PV inverters. IEEE Trans Power Syst 2013;28(3):3429–39.
[7] Li Huijuan, Li Fangxing, Xu Yan, Rizy D Tom, Adhikari Sarina. Autonomous and adaptive voltage control using multiple distributed energy resources. IEEE Trans Power Syst 2012;28(2):718–30.
[8] Turitsyn Konstantin, Sulc Petr, Backhaus Scott, Chertkov Michael. Options for control of reactive power by distributed photovoltaic generators. Proc IEEE 2011;99(6):1063–73.
[9] Niknam Taher, Firouzi Bahman Bahmani, Ostadi Amir. A new fuzzy adaptive particle swarm optimization for daily Volt/Var control in distribution networks considering distributed generators. Appl Energy 2010;87(6):1919–28.
[10] Calderaro Vito, Conio Gaspare, Galdi Vincenzo, Massa Giovanni, Piccolo Antonio. Optimal decentralized voltage control for distribution systems with inverter-based distributed generators. IEEE Trans Power Syst 2013;29(1):230–41.
[11] Antunes Carlos Henggeler, Pires Dulce Fernão, Barrico Carlos, Gomes Alvaro, Martins António Gomes. A multi-objective evolutionary algorithm for reactive power compensation in distribution networks. Appl Energy 2009;86(7–8):977–84.
[12] Feng Changsen, Li Zhiyi, Shahidehpour Mohammad, Wen Fushuan, Liu Weijia, Wang Xiaolei. Decentralized short-term voltage control in active power distribution systems. IEEE Trans Smart Grid 2017;9(5):4566–76.
[13] Cheng Lin, Chang Yao, Huang Renle. Mitigating voltage problem in distribution system with distributed solar generation using electric vehicles. IEEE Trans Sustain Energy 2015;6(4):1475–84.
[14] Mokgonyana Lesiba, Zhang Jiangfeng, Zhang Lijun, Xia Xiaohua. Coordinated two-stage volt/var management in distribution networks. Electr Power Syst Res 2016;141:157–64.
[15] Zhang Qianzhi, Dehghanpour Kaveh, Wang Zhaoyu. Distributed CVR in unbalanced distribution systems with PV penetration. IEEE Trans Smart Grid 2018;10(5):5308–19.
[16] Kekatos Vassilis, Wang Gang, Conejo Antonio J, Giannakis Georgios B. Stochastic reactive power management in microgrids with renewables. IEEE Trans Power Syst 2014;30(6):3386–95.
[17] Zhou Bin, Xu Da, Chan Ka Wing, Li Canbing, Cao Yijia, Bu Siqi. A two-stage framework for multiobjective energy management in distribution networks with a high penetration of wind energy. Energy 2017;135:754–66.
[18] Nazir Firdous Ul, Pal Bikash C, Jabr Rabih A. A two-stage chance constrained volt/var control scheme for active distribution networks with nodal power uncertainties. IEEE Trans Power Syst 2018;34(1):314–25.
[19] Balram Pavan, Carlson Ola, et al. Comparative study of MPC based coordinated voltage control in LV distribution systems with photovoltaics and battery storage. Int J Electr Power Energy Syst 2018;95:227–38.
[20] Guo Yifei, Wu Qiuwei, Gao Houlei, Chen Xinyu, Østergaard Jacob, Xin Huanhai. MPC-based coordinated voltage regulation for distribution networks with distributed generation and energy storage system. IEEE Trans Sustain Energy 2018;10(4):1731–9.

[21] Wang Zhaoyu, Wang Jianhui, Chen Bokan, Begovic Miroslav M, He Yanyi. MPC-based voltage/var optimization for distribution circuits with distributed generators and exponential load models. IEEE Trans Smart Grid 2014;5(5):2412–20.
[22] Jiang Yibao, Wan Can, Wang Jianhui, Song Yonghua, Dong Zhao Yang. Stochastic receding horizon control of active distribution networks with distributed renewables. IEEE Trans Power Syst 2018;34(2):1325–41.
[23] Ghosh Shibani, Rahman Saifur, Pipattanasomporn Manisa. Distribution voltage regulation through active power curtailment with PV inverters and solar generation forecasts. IEEE Trans Sustain Energy 2016;8(1):13–22.
[24] Baran Mesut E, Wu Felix F. Network reconfiguration in distribution systems for loss reduction and load balancing. IEEE Power Eng Rev 1989;9(4):101–2.
[25] Zhu Hao, Liu Hao Jan. Fast local voltage control under limited reactive power: Optimality and stability analysis. IEEE Trans Power Syst 2015;31(5):3794–803.
[26] Bapat Ravindra B. Graphs and Matrices, Vol. 27. Springer; 2010.
[27] Niknam Taher, Zare Mohsen, Aghaei Jamshid. Scenario-based multiobjective volt/var control in distribution networks including renewable energy sources. IEEE Trans Power Deliv 2012;27(4):2004–19.
[28] Wu Lei, Shahidehpour Mohammad, Li Tao. Stochastic security-constrained unit commitment. IEEE Trans Power Syst 2007;22(2):800–11.
[29] GAMS/SCENRED2 documentation.
[30] Nick Mostafa, Cherkaoui Rachid, Paolone Mario. Optimal allocation of dispersed energy storage systems in active distribution networks for energy balance and grid support. IEEE Trans Power Syst 2014;29(5):2300–10.
[31] Venkatesh B, Chandramohan S, Kayalvizhi N, Devi RP Kumudini. Optimal reconfiguration of radial distribuion system using artificial intelligence methods. In: 2009 IEEE Toronto International Conference Science and Technology for Humanity (TIC-STH). IEEE; 2009, p. 660–5.
[32] Löfberg J. YALMIP : A Toolbox for Modeling and Optimization in MATLAB, In: Proceedings of the CACSD Conference, 2004: Taipei, Taiwan;.
[33] Gurobi Optimization LLC. Gurobi optimizer reference manual. 2020, http://www.gurobi.com.
[34] National Renewable Energy Laboratory (NREL), https://www.nrel.gov/grid/solar-resource/renewable-resource-data.html.
[35] Li Peng, Ji Haoran, Wang Chengshan, Zhao Jinli, Song Guanyu, Ding Fei, Wu Jianzhong. Coordinated control method of voltage and reactive power for active distribution networks based on soft open point. IEEE Trans Sustain Energy 2017;8(4):1430–42.
[36] Wang Zhaoyu, Chen Hao, Wang Jianhui, Begovic Miroslav. Inverter-less hybrid voltage/var control for distribution circuits with photovoltaic generators. IEEE Trans Smart Grid 2014;5(6):2718–28.
[37] Wong TK, Mak CM, Chung TS. Co-ordination of transformer tap and capacitor operation for reactive power voltage control in a distribution primary substation. 2000.